Uncertainty Quantification and Control During Mars Powered Descent and Landing using Covariance Steering

Jack Ridderhof* and Panagiotis Tsiotras †

Georgia Institute of Technology, Atlanta, GA, 30332, USA

We consider the design of a feedback control for a stochastic affine time-varying system with explicit boundary conditions on the state mean and covariance, a method referred to in the literature as covariance steering, with application to the Martian powered descent problem. Linear covariance steering theory is first extended to include a deterministic affine forcing term, and is then simulated with disturbances on the order of those expected for a typical Martian entry, descent, and landing mission. Numerical results demonstrate the benefits of the approach compared to standard Monte Carlo evaluation.

I. Introduction

Entry, Descent, and Landing (EDL) is the process of guiding a spacecraft entering a planet's atmosphere, decelerating from orbit, and descending to a safe landing site on the planet's surface. Atmospheric disturbances, localization error, and other factors contribute to substantial deviations from the nominal descent trajectory. These factors must be accounted for when selecting a landing target. During the powered flight segment of EDL, which spans from the end of aerodynamic deceleration to touchdown, it is required to control deviated trajectories to a safe landing site, while removing the remaining kinetic energy. Divert radius, namely, the distance from the uncontrolled touchdown point to the target touchdown point, is an important design parameter when selecting a landing site. Improvements in powered descent guidance divert capabilities will allow future missions to select more scientifically "interesting" landing sites, also opening the possibility of resupply missions for human outposts.[1]

The first American system to land on Mars, the Viking I, which landed on July 20, 1976, used a gravity turn guidance scheme for terminal descent,[2] namely, the thrust vector was directed opposite of the velocity vector. During this phase, the Viking I guidance computer tracked steering commands to achieve the gravity turn while maintaining a programmed descent rate profile until a touchdown with an approximate vertical velocity of 2.4 m/s,.[2] The Viking EDL system achieved a 280 km by 100 km 3σ landing ellipse. The Mars Path Finder (MPF) mission, in contrast to the Viking mission, did not track a closed-loop descent profile during powered descent, but rather relied on an altitude-triggered firing of solid rockets coupled with an airbag system designed for a 12.5 m/s vertical velocity and maximum of a 20 m/s horizontal velocity at touchdown.[3,4] The subsequent Mars Exploration Rover missions used a variation of the MPF EDL scheme,[4] and the Phoenix mission used a variation of the Viking gravity turn guidance for terminal descent.[5]

The most sophisticated Martian EDL procedure to date was performed by the Mars Science Laboratory (MSL) mission. The 1,500 kg MSL spacecraft began powered descent at an altitude of 1.6 km with a velocity of 85 m/s.[6] The Apollo era fifth-order polynomial guidance scheme[7] was used to target a point 242 m above the landing site and 300 m perpendicular to the entry trajectory plane before initiating the final vertical descent to the surface.[6,8] The total time of the flight segment was determined as a function of the initial altitude, which was in turn selected off-line in order to satisfy the maximum acceleration constraint.[7] The polynomial trajectory was computed by the flight computer at the start of the powered descent phase and was subsequently tracked by a reference path following program.[7] The MSL achieved a 20 km by 20 km 3σ landing ellipse, nearly an order of magnitude greater than the Viking lander.

*Graduate Student, Department of Aerospace Engineering, Georgia Institute of Technology, Atlanta, GA, 30332, USA.

†Dean's Professor, School of Aerospace Engineering, and Institute for Robotics and Intelligent Machines, AIAA Fellow.

On the theoretical side, several previous works have addressed the powered descent problem, using primarily optimization techniques. One proposed method solves the two-point boundary value problem with an 11^{th} degree polynomial approximation and a parametric optimizer subject to control and path constraints.[9] However, the optimization cannot be performed onboard due to computational time constraints. Most recently, it has been shown that convex optimization is a promising strategy for solving optimal powered descent trajectories.[10] Since a convex optimization program can be guaranteed to converge to the unique solution, it is suitable for on-line implementation, by which the optimal trajectory to follow is computed continuously, on-the-fly, during descent. The 2015 NASA Technology Roadmap specifically cites convex optimization as a potential next-generation solution to the divert guidance problem.[1]

This work considers uncertainty and dispersion of EDL trajectories by modeling the system as a stochastic differential equation, and by controlling its mean state and covariance using covariance steering, which is a theory for controlling the state covariance of stochastic systems. Recent works have shown that, for a linear time-varying system subject to Gaussian white noise, the state covariance is controllable through selection of a full-state feedback gain,[11] and furthermore, state mean and covariance may explicitly be provided as an end-point constraint for an optimal feedback design.[12] By applying covariance steering theory to EDL, the state mean and covariance of descent trajectories are used as boundary conditions to solve for the optimal time-varying controller gains. This approach would allow a system designer to specify the first and second moments of the desired distribution of trajectories as constraints when designing a feedback strategy, rather than iteratively tuning gains by trial and error, running simulations and making corrections, thus reducing extensive Monte Carlo validation studies.

In this paper, linear covariance steering theory is first extended for application to the EDL problem. An affine forcing term is added to the system to model gravitational acceleration, and a scalar multiplier on the noise magnitude is added to the governing stochastic differential equation to model the actual effect of noise. Then, the nonlinear dynamics governing powered descent are relaxed to an affine time-varying model by replacing the mass flow dynamics with a predetermined time-varying mass profile, which is selected through an iteration scheme. The controller gains that are solved using the simplified mass profile are shown to successfully steer the nonlinear system during powered descent. The theory is then used in Monte Carlo simulations of several powered descent diversion maneuvers using a point-mass spacecraft model to validate the proposed covariance steering controller.

II. Problem Formulation

We consider the problem of guiding a spacecraft during powered descent from an initial position and velocity to a soft landing (zero vertical and lateral velocity at touchdown). The spacecraft is modeled as a point-mass with position vector $r \in \mathbb{R}^3$ in a surface-fixed frame, which will be assumed inertial. Neglecting aerodynamic forces, the equation of motion is

$$\ddot{r} = g + u/m, \tag{1}$$

where $g \in \mathbb{R}^3$ denotes the gravitational acceleration, $u \in \mathbb{R}^3$ is the control thrust, and m is the spacecraft mass, which changes proportionally to thrust magnitude by

$$\dot{m} = -\alpha \|u\|, \tag{2}$$

where $\alpha > 0$. However, for the purposes of the following analysis, the mass m in Eq. (1) will be assumed to be given *a priori* as a function of time. In Sections IV and V we show that by iterating on the selection of the mass profile $m(t)$, the proposed control scheme is successful even when simulated with the actual dynamics in Eqs. (1) and (2).

Defining the state vector as

$$x = \begin{bmatrix} x_1 \\ x_2 \end{bmatrix} = \begin{bmatrix} r \\ \dot{r} \end{bmatrix} \in \mathbb{R}^6, \tag{3}$$

the dynamics assume the state-space form

$$\begin{bmatrix} \dot{x}_1 \\ \dot{x}_2 \end{bmatrix} = \begin{bmatrix} 0 & I \\ 0 & 0 \end{bmatrix} \begin{bmatrix} x_1 \\ x_2 \end{bmatrix} + \begin{bmatrix} 0 \\ I/m \end{bmatrix} u + \begin{bmatrix} 0 \\ g \end{bmatrix},$$

where I is the identity matrix. These equations are of the form

$$\dot{x} = A(t)x + B(t)u + c(t), \tag{4}$$

where $A(t) \in \mathbb{R}^{n\times n}$, $B(t) \in \mathbb{R}^{n\times m}$ are prescribed matrices for all $t \geq 0$ and $c(t) \in \mathbb{R}^n$. Disturbances and uncertainty affecting Eq. (4) can be modeled as noise acting on the system, yielding the stochastic system

$$\mathrm{d}x = A(t)x\mathrm{d}t + B(t)u\mathrm{d}t + c(t)\mathrm{d}t + \gamma B(t)\mathrm{d}w, \tag{5}$$

where $\{w(t), t \in [0,T]\}$ is an m-dimensional Brownian motion, and $\gamma > 0$ is a metric of the relative magnitude of noise to control. As $\gamma \to 0$, the system in Eq. (5) reduces to Eq. (4), hence γ may be used to tune the expected noise magnitude.

The solution of Eq. (5) yields a stochastic process $x(t)$ where, for each $t \geq 0$, $x(t)$ is a random variable with mean $\bar{x}(t)$ and covariance $\Sigma(t)$, that is,

$$\bar{x}(t) = \mathbb{E}[x(t)], \tag{6}$$

and

$$\Sigma(t) = \mathbb{E}[(x(t) - \bar{x}(t))(x(t) - \bar{x}(t))^{\intercal}]. \tag{7}$$

We assume finite-time problems where $t \in [0,T]$ with the final time $T \geq 0$ fixed. The boundary conditions are given by

$$\bar{x}(0) = \bar{x}_0, \qquad \bar{x}(T) = \bar{x}_T, \tag{8}$$

$$\Sigma(0) = \Sigma_0, \qquad \Sigma(T) = \Sigma_T. \tag{9}$$

Let the performance measure associated with the system in Eq. (5) be given by

$$J(u) = \mathbb{E}[\int_0^T u^{\intercal}(t)u(t)\mathrm{d}t]. \tag{10}$$

The stochastic optimal control problem is then to minimize Eq. (10) subject to dynamics in Eq. (5), and boundary conditions in Eqs. (8), (9).

III. Covariance Steering

To find a candidate optimal control, co-state variables Λ and λ will be used to construct an equivalent performance measure, under which a minimizing selection of u will be clear. Let $\Lambda : [0,T] \to \mathbb{R}^{n\times n}$, $\Lambda \in C^1$, $\Lambda(t) = \Lambda^{\intercal}(t)$ for all $t \in [0,T]$ be a matrix-valued function, and let $\lambda : [0,T] \to \mathbb{R}^n$, $\lambda \in C^1$. Then,

$$\begin{aligned}
\mathbb{E}[x^{\intercal}(t)\Lambda(t)x(t)] &= \mathbb{E}[x^{\intercal}(t)\Lambda(t)x(t)] + \bar{x}^{\intercal}(t)\Lambda(t)\bar{x}(t) - \bar{x}^{\intercal}(t)\Lambda(t)\bar{x}(t) && (11)\\
&= \mathbb{E}[x^{\intercal}(t)\Lambda(t)x(t) - 2x^{\intercal}(t)\Lambda(t)\bar{x}(t) + \bar{x}^{\intercal}(t)\Lambda(t)\bar{x}(t)] + \bar{x}^{\intercal}(t)\Lambda(t)\bar{x}(t) && (12)\\
&= \mathbb{E}[(x(t) - \bar{x}(t))^{\intercal}\Lambda(t)(x(t) - \bar{x}(t))] + \bar{x}^{\intercal}(t)\Lambda(t)\bar{x}(t) && (13)\\
&= \mathbb{E}[\mathrm{tr}(\Lambda(t)(x(t) - \bar{x}(t))(x(t) - \bar{x}(t))^{\intercal})] + \bar{x}^{\intercal}(t)\Lambda(t)\bar{x}(t) && (14)\\
&= \mathrm{tr}(\Lambda(t)\mathbb{E}[(x(t) - \bar{x}(t))(x(t) - \bar{x}(t))^{\intercal}]) + \bar{x}^{\intercal}(t)\Lambda(t)\bar{x}(t) && (15)\\
&= \mathrm{tr}(\Lambda(t)\Sigma(t)) + \bar{x}^{\intercal}(t)\Lambda(t)\bar{x}(t), && (16)
\end{aligned}$$

and

$$\mathbb{E}[\lambda^{\intercal}(t)x(t)] = \lambda^{\intercal}(t)\bar{x}(t). \tag{17}$$

Because the end-point state mean and covariance are both fixed, the values in Eqs. (16) and (17) are constant at times $t = 0$ and $t = T$, and are determined by the boundary conditions. Thus, minimizing Eq. (10) over variations of u is equivalent to minimizing the modified index

$$\tilde{J}(u) = \mathbb{E}\big[\int_0^T u^{\intercal}(t)u(t)\mathrm{d}t + x^{\intercal}(T)\Lambda(T)x(T) - x^{\intercal}(0)\Lambda(0)x(0) - 2\lambda^{\intercal}(T)x(T) + 2\lambda^{\intercal}(0)x(0)\big], \tag{18}$$

which is equivalent to

$$\tilde{J}(u) = \mathbb{E}\big[\int_0^T u^{\intercal}(t)u(t)\mathrm{d}t + \int_0^T \mathrm{d}(x^{\intercal}(t)\Lambda(t)x(t) - 2\lambda^{\intercal}(t)x(t))\big]. \tag{19}$$

Expanding the second integral in Eq. (19) and using Itô's rule, one obtains

$$\tilde{J}(u) = \mathbb{E}\bigg[\int_0^T u^\intercal(t)u(t)\mathrm{d}t + \int_0^T \big[x^\intercal(t)\dot{\Lambda}(t)x(t) - 2\dot{\lambda}^\intercal(t)x(t) + (A(t)x + B(t)u + c(t))^\intercal\Lambda(t)x(t)$$
$$+ x^\intercal(t)\Lambda(t)(A(t)x + B(t)u + c(t)) - 2\lambda^\intercal(t)(A(t)x + B(t)u + c(t))$$
$$+ \gamma^2\mathrm{tr}(\Lambda(t)B(t)B^\intercal(t))\big]\mathrm{d}t + 2\gamma\int_0^T \big(x(t)\Lambda(t)B(t) - \lambda^\intercal(t)B(t)\big)\mathrm{d}w\bigg] \quad (20)$$

Because $w(t)$ is a zero-mean process, the expectation of the last integral over $\mathrm{d}w$ is zero. Furthermore, if Λ satisfies the matrix Riccati equation

$$\dot{\Lambda} = -A^\intercal(t)\Lambda - \Lambda A(t) + \Lambda B(t)B^\intercal(t)\Lambda, \quad (21)$$

for all $t \in [0, T]$, and λ satisfies the affine differential equation

$$\dot{\lambda} = -(A(t) - B(t)B^\intercal(t)\Lambda(t))^\intercal\lambda + \Lambda(t)c(t), \quad (22)$$

for all $t \in [0, T]$, then Eq. (20) reduces to

$$\tilde{J}(u) = \mathbb{E}\bigg[\int_0^T \|u(t) + B^\intercal(t)\Lambda(t)x(t) - B^\intercal(t)\lambda(t)\|^2\mathrm{d}t + \gamma^2\int_0^T \mathrm{tr}(\Lambda(t)B(t)B^\intercal(t))\mathrm{d}t\bigg]. \quad (23)$$

Because the second integral is constant over variations of u, the candidate optimal control

$$u^*(x, t) = -B^\intercal(t)\Lambda(t)x + B^\intercal(t)\lambda(t), \quad (24)$$

minimizes Eq. (23), and hence it also minimizes Eq. (10). The optimal evolution of the system in Eq. (5) with respect to the performance index in Eq. (10) is thus

$$\mathrm{d}x = (A(t) - B(t)B^\intercal(t)\Lambda(t))x\mathrm{d}t + B(t)B^\intercal(t)\lambda(t)\mathrm{d}t + c(t)\mathrm{d}t + \gamma B(t)\mathrm{d}w. \quad (25)$$

We now proceed to find the boundary conditions $\Lambda(0)$, $\lambda(0)$ such that Eq. (25) satisfies the mean and covariance boundary conditions in Eqs. (8) and (9). From Eq. (22) it follows that $\lambda(t)$ has the solution

$$\lambda(t) = \bar{\Theta}(t, 0)\lambda(0) + \int_0^t \bar{\Theta}(t, \tau)\Lambda(\tau)c(\tau)\,\mathrm{d}\tau, \quad (26)$$

where $\bar{\Theta} : [0, T] \times [0, T] \to \mathbb{R}^{n\times n}$ is the transition matrix having the properties

$$\frac{\partial\bar{\Theta}(t, s)}{\partial t} = -(A(t) - B(t)B^\intercal(t)\Lambda(t))^\intercal\bar{\Theta}(t, s), \qquad \bar{\Theta}(s, s) = I. \quad (27)$$

Let the transition matrix $\Theta : [0, T] \times [0, T] \to \mathbb{R}^{n\times n}$, which obeys

$$\frac{\partial\Theta(t, s)}{\partial t} = (A(t) - B(t)B^\intercal(t)\Lambda(t))\Theta(t, s), \qquad \Theta(s, s) = I. \quad (28)$$

Then, since

$$\Theta(t, s) = \bar{\Theta}^\intercal(s, t) = \bar{\Theta}^{-\intercal}(t, s), \quad (29)$$

it follows that

$$\lambda(t) = \Theta^\intercal(0, t)\lambda(0) + \int_0^t \Theta^\intercal(\tau, t)\Lambda(\tau)c(\tau)\,\mathrm{d}\tau. \quad (30)$$

By taking the expectation of Eq. (25) and dividing by $\mathrm{d}t$, it follows that $\bar{x}$ obeys the equation

$$\dot{\bar{x}} = (A(t) - B(t)B^\intercal(t)\Lambda(t))\bar{x} + B(t)B^\intercal(t)\lambda(t) + c(t), \quad (31)$$

and therefore it has the solution

$$\bar{x}(t) = \Theta(t, 0)\bar{x}(0) + \int_0^t \Theta(t, \tau)B(\tau)B^\intercal(\tau)\lambda(\tau)\mathrm{d}\tau + \int_0^t \Theta(t, \tau)c(\tau)\,\mathrm{d}\tau. \quad (32)$$

Substituting $\lambda(t)$ from Eq. (30) yields

$$\bar{x}(t) = \Theta(t,0)\bar{x}(0) + \int_0^t \Theta(t,\tau)B(\tau)B^{\intercal}(\tau)\left[\Theta^{\intercal}(0,\tau)\lambda(0) + \int_0^{\tau} \Theta^{\intercal}(\sigma,\tau)\Lambda(\sigma)c(\sigma)\mathrm{d}\sigma\right]\mathrm{d}\tau + \int_0^t \Theta(t,\tau)c(\tau)\mathrm{d}\tau. \quad (33)$$

and at time $t = T$,

$$\bar{x}(T) = \Theta(T,0)\bar{x}(0) + \int_0^T \Theta(T,\tau)B(\tau)B^{\intercal}(\tau)\Theta^{\intercal}(0,\tau)\lambda(0)\mathrm{d}\tau + \int_0^T \Theta(T,\tau)B(\tau)B^{\intercal}(\tau)\left[\int_0^{\tau} \Theta^{\intercal}(\sigma,\tau)\Lambda(\sigma)c(\sigma)\mathrm{d}\sigma\right]\mathrm{d}\tau + \int_0^T \Theta(T,\tau)c(\tau)\,\mathrm{d}\tau. \quad (34)$$

Let

$$c_1 = \int_0^T \Theta(T,\tau)B(\tau)B^{\intercal}(\tau)\left[\int_0^{\tau} \Theta^{\intercal}(\sigma,\tau)\Lambda(\sigma)c(\sigma)\mathrm{d}\sigma\right]\mathrm{d}\tau, \quad (35)$$

and

$$c_2 = \int_0^T \Theta(T,\tau)c(\tau)\,\mathrm{d}\tau. \quad (36)$$

Solving for $\lambda(0)$ then yields

$$\lambda(0) = \left[\int_0^T \Theta(T,\tau)B(\tau)B^{\intercal}(\tau)\Theta^{\intercal}(0,\tau)\mathrm{d}\tau\right]^{-1}\big(\bar{x}(T) - \Theta(T,0)\bar{x}(0) - c_1 - c_2\big). \quad (37)$$

Define the controllability Gramian of the closed-loop system in Eq. (31) as

$$\tilde{M}(T,0) = \int_0^T \Theta(T,\tau)B(\tau)B^{\intercal}(\tau)\Theta^{\intercal}(T,\tau)\mathrm{d}\tau. \quad (38)$$

Using Eq. (38), the expression for $\lambda(0)$ from Eq. (37) leads to

$$\lambda(0) = \Theta^{\intercal}(T,0)\tilde{M}^{-1}(T,0)\big(\bar{x}(T) - \Theta(T,0)\bar{x}(0) - c_1 - c_2\big). \quad (39)$$

Next, we solve for $\Lambda(0)$ such that $\Sigma(0) = \Sigma_0$ and $\Sigma(T) = \Sigma_T$. From Itô's rule, the evolution of the state covariance for the system in Eq. (25) is given by

$$\dot{\Sigma} = (A(t) - B(t)B^{\intercal}(t)\Lambda(t))\Sigma + \Sigma(A(t) - B(t)B^{\intercal}(t)\Lambda(t))^{\intercal} + \gamma^2 B(t)B^{\intercal}(t). \quad (40)$$

Following the procedure in Ref. [12], introduce $H : [0,T] \to \mathbb{R}^{n\times n}$ by $H(t) = \gamma^2\Sigma^{-1}(t) - \Lambda(t)$. Then

$$\dot{H} = -\gamma^2\Sigma^{-1}(t)\dot{\Sigma}(t)\Sigma^{-1}(t) - \dot{\Lambda}(t), \quad (41)$$

which, after substituting Eqs. (21) and (40), reduces to

$$\dot{H} = -HA(t) - A^{\intercal}(t)H - HB(t)B^{\intercal}(t)H, \quad (42)$$

with the boundary conditions

$$H(0) = \gamma^2\Sigma^{-1}(0) - \Lambda(0), \qquad H(T) = \gamma^2\Sigma^{-1}(T) - \Lambda(T). \quad (43)$$

Define $Q(t) = \Lambda^{-1}(t)$ and $P(t) = H^{-1}(t)$. Then it can be easily shown that

$$\dot{Q} = A(t)Q + QA^{\intercal}(t) - B(t)B^{\intercal}(t), \quad (44)$$

and

$$\dot{P} = A(t)P + PA^{\intercal}(t) + B(t)B^{\intercal}(t), \quad (45)$$

with the boundary conditions

$$\Sigma^{-1}(0) = \gamma^2(P^{-1}(0) + Q^{-1}(0)), \qquad \Sigma^{-1}(T) = \gamma^2(P^{-1}(T) + Q^{-1}(T)). \tag{46}$$

Let the open-loop transition matrix $\Phi : [0,T] \times [0,T] \to \mathbb{R}^{n\times n}$, which obeys

$$\frac{\partial \Phi(t,s)}{\partial t} = A(t)\Phi(t,s), \qquad \Phi(s,s) = I, \tag{47}$$

and let the controllability Gramian of the open-loop system be given by

$$M(T,0) = \int_0^T \Phi(T,\tau)B(\tau)B^\intercal(\tau)\Phi^\intercal(T,\tau)\mathrm{d}\tau. \tag{48}$$

Then the initial value $Q(0)$ can be solved for with Algorithm 1, which yields $Q(t)$ invertible for all $t \in [0,T]$.[12] Since $\Lambda(0) = Q^{-1}(0)$, $\Lambda(t)$ is obtained by integrating Eq. (21) forward. Then the closed-loop state transition matrix $\Theta(t,s)$ can be numerically solved from Eq. (28) and used to compute $\lambda(0)$ from Eq. (39), and $\lambda(t)$ is solved by integrating Eq. (22) forward. The solution procedure is summarized in Algorithm 2.

Algorithm 1 Iteration to find $Q(0)$ and $P(0)$ that satisfy the boundary conditions in Eq. (46).[12]

function CALCULATEINITIALQ$(\Phi(t,s), M(T,0), \gamma, \Sigma_0, \Sigma_T, T)$
  $P(0) \leftarrow I$
  $Q(0) \leftarrow I$
  $tol \leftarrow$ some small number > 0
  repeat
    $P(T) \leftarrow \Phi(T,0)P(0)\Phi(T,0)^\intercal + M(T,0)$
    $Q(T) \leftarrow ((\gamma\Sigma_T)^{-1} - P^{-1}(T))^{-1}$
    $Q(0)_{\text{new}} \leftarrow \Phi(0,T)(Q(T) + M(T,0))\Phi(0,T)^\intercal$
    $P(0)_{\text{new}} \leftarrow ((\gamma\Sigma_0)^{-1} - Q^{-1}(0))^{-1}$
    $dQ(0) \leftarrow Q(0)_{\text{new}} - Q(0)$
    $dP(0) \leftarrow P(0)_{\text{new}} - P(0)$
    $Q(0) \leftarrow Q(0)_{\text{new}}$
    $P(0) \leftarrow P(0)_{\text{new}}$
  until $\|dQ(0)\| < tol$ and $\|dP(0)\| < tol$
  return $Q(0)$

Algorithm 2 Procedure to find covariance steering controller gains.

function COVARIANCESTEERING$(A(t), B(t), c(t), \gamma, \Phi(t,s), \bar{x}_0, \bar{x}_T, \Sigma_0, \Sigma_T, T)$
  $M(T,0) \leftarrow$ Evaluate Eq. (48)
  $Q(0) \leftarrow$ `CalculateInitialQ`$(\Phi(t,s), M(T,0), \gamma, \Sigma_0, \Sigma_T, T)$
  $\Lambda(0) \leftarrow Q^{-1}(0)$
  $\Lambda(t) \leftarrow$ Integrate Eq. (21) with $\Lambda(0)$ from 0 to T
  $\Theta(t,s) \leftarrow$ Integrate Eq. (28)
  $\tilde{M}(T,0) \leftarrow$ Evaluate Eq. (38)
  $\lambda(0) \leftarrow$ Evaluate Eq. (39) with $\Theta(t,s)$ and $\tilde{M}(T,0)$
  $\lambda(t) \leftarrow$ Integrate Eq. (22) with $\lambda(0)$ from 0 to T
  $u(x,t) \leftarrow -B^\intercal(t)\Lambda(t)x + B^\intercal(t)\lambda(t)$
  return $u(x,t)$

IV. Successive Linearization Approach

Because covariance steering theory cannot be directly applied to nonlinear systems, the system in Eqs. (1) and (2) is linearized about a mass profile $m(t)$, which reduces the system to the time-varying affine system in Eq. (4). The mass profile is obtained through the iterative application of covariance steering and subsequent simulation of the closed-loop nonlinear system, which is summarized in Algorithm 3. Figure 1 shows the iteration scheme converging when applied to the scenario presented in Section V. Furthermore, in Section V, we show that if the *prior* mass profile is close enough to the *posterior* mass profile, as determined by evaluation of Eqs. (1) and (2), then the control scheme generated from the preceding analysis is sufficient to guide the system in Eqs. (1) and (2) to the target state mean and covariance.

Algorithm 3 Procedure to find the mass profile for a powered descent with covariance steering.

function IDENTIFYMASSPROFILE($\gamma, \bar{x}_0, \bar{x}_T, \Sigma_0, \Sigma_T, T$)
  $A \leftarrow \begin{bmatrix} 0 & I \\ 0 & 0 \end{bmatrix}$
  $\Phi(t,s) = \exp(A(t-s))$
  $c \leftarrow \begin{bmatrix} 0 & g \end{bmatrix}^\intercal$
  $m(t) \leftarrow m_{\text{wet}}$
  repeat
    $m'(t) \leftarrow m(t)$
    $B(t) \leftarrow \begin{bmatrix} 0 & I \end{bmatrix}^\intercal / m'(t)$
    $u(x,t) \leftarrow$ `CovarianceSteering`$(A, B(t), c, \gamma, \Phi(t,s), \bar{x}_0, \bar{x}_T, \Sigma_0, \Sigma_T, T)$
    $z_0 \leftarrow \begin{bmatrix} \bar{x}_0^\intercal & m_{\text{wet}} \end{bmatrix}^\intercal$
    $m(t) \leftarrow$ `SimulateNonlinearDynamics`$(z_0, u(x,t))$
  until `IntegrateDifference`$(m(t), m'(t)) <$ Tolerance
  return $m(t)$

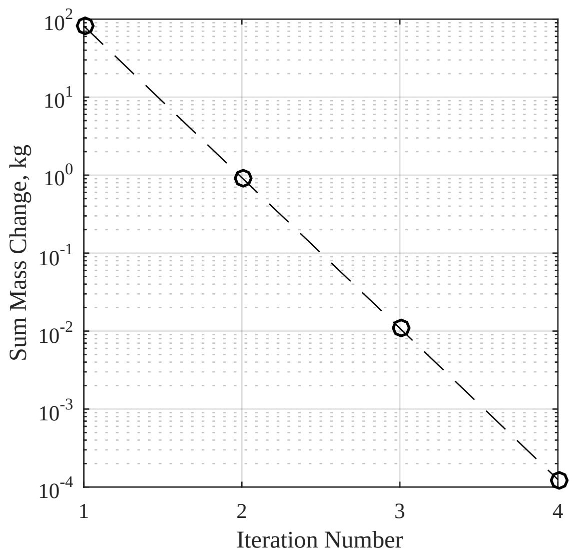

Figure 1. Differences in mass profiles between iterations of the mass profile approximation procedure with the change in mass between iterations given on a log scale.

V. Numerical Simulations

The performance of the proposed covariance steering controller is evaluated in a two-dimensional simulation of a Martian powered descent involving two sequential divert maneuvers, whose geometry is shown in Figure 2. Time-varying control gains were determined by an initial, intermediate, and final state mean and covariance, hence the performance of the control scheme after passing the intermediate target is dependent on the mean and covariance of the system state at the intermediate target. That is, if the trajectories disperse beyond the end-point covariance requirement, the controller gains scheduled after the intermediate target will be insufficient to meet the final covariance target. This scenario demonstrates the benefit of the covariance steering approach to guarantee the mean and covariance of trajectories at some prescribed time without the need to iteratively tune cost weights. Note that while the final time is fixed in this formulation, the free final time problem can be solved by conducting a line search over final time.

In these simulations, the nonlinear system in Eqs. (1) and (2) was modified to include noise in the control channel as follows

$$\mathrm{d}\dot{r} = (g + u/m)\mathrm{d}t + (\gamma/m)I\mathrm{d}w, \tag{49}$$

where $\gamma = 0.02$, and the two-dimensional state vector is

$$x = \begin{bmatrix} r_1 & r_2 & \dot{r}_1 & \dot{r}_2 \end{bmatrix}^\intercal, \tag{50}$$

where r_1 and r_2 are the downrange position and altitude respectively. The initial, intermediate, and target spacecraft mean positions and covariances are, respectively,

$$\bar{x}_0 = \begin{bmatrix} 250 \text{ m} \\ 500 \text{ m} \\ 50\sin 70^\circ \text{ m/s} \\ 50\cos 70^\circ \text{ m/s} \end{bmatrix}, \quad \Sigma_0 = \begin{bmatrix} 40 \text{ m}^2 & 0 & 0 & 0 \\ 0 & 40 \text{ m}^2 & 0 & 0 \\ 0 & 0 & 5 \text{ (m/s)}^2 & 0 \\ 0 & 0 & 0 & 5 \text{ (m/s)}^2 \end{bmatrix} \tag{51}$$

$$\bar{x}_{TI} = \begin{bmatrix} 50 \text{ m} \\ 150 \text{ m} \\ 0 \text{ m/s} \\ -5 \text{ m/s} \end{bmatrix}, \quad \Sigma_{TI} = \begin{bmatrix} 10 \text{ m}^2 & 0 & 0 & 0 \\ 0 & 10 \text{ m}^2 & 0 & 0 \\ 0 & 0 & 1 \text{ (m/s)}^2 & 0 \\ 0 & 0 & 0 & 1 \text{ (m/s)}^2 \end{bmatrix} \tag{52}$$

$$\bar{x}_{TF} = \begin{bmatrix} 100 \text{ m} \\ 50 \text{ m} \\ 0 \text{ m/s} \\ 0 \text{ m/s} \end{bmatrix}, \quad \Sigma_{TF} = \begin{bmatrix} 5 \text{ m}^2 & 0 & 0 & 0 \\ 0 & \frac{1}{4} \text{ m}^2 & 0 & 0 \\ 0 & 0 & \frac{1}{4} \text{ (m/s)}^2 & 0 \\ 0 & 0 & 0 & \frac{1}{4} \text{ (m/s)}^2 \end{bmatrix}, \tag{53}$$

and the time for from initialization to the intermediate target is 26 seconds. The time from the intermediate to final target is 15 seconds. The spacecraft wet mass is 1,500 kg, maximum thrust is 18,000 N, specific impulse is 210 s, which gives $\alpha = 4.85\text{e}{-4}$ kg/Ns, and gravitational acceleration is 3.71 m/s^2. A total of 2,000 trials were simulated on a computing cluster for 12 hours using 32 cores. Over the 2,000 trials, the final state mean and covariance were

$$\bar{x}_{TF,\text{sim}} = \begin{bmatrix} 100.111 \\ 49.807 \text{ m} \\ 0.092 \text{ m/s} \\ -0.005 \text{ m/s} \end{bmatrix}, \quad \Sigma_{TF,\text{sim}} = \begin{bmatrix} 3.889 \text{ m}^2 & -0.055 \text{ m}^2 & 0.036 \text{ m}^2/\text{s} & -0.009 \text{ m}^2/\text{s} \\ -0.552 \text{ m}^2 & 0.250 \text{ (m/s)}^2 & 0.013 \text{ m}^2/\text{s} & 0.011 \text{ m}^2/\text{s} \\ 0.036 \text{ m}^2/\text{s} & 0.013 \text{ m}^2/\text{s} & 0.243 \text{ (m/s)}^2 & -0.007 \text{ (m/s)}^2 \\ -0.009 \text{ m}^2/\text{s} & 0.010 \text{ m}^2/\text{s} & -0.006 \text{ (m/s)}^2 & 0.276 \text{ (m/s)}^2 \end{bmatrix}, \tag{54}$$

and the mean final mass was 1,349 kg, compared to 1,346 kg predicted by the prior mass profile.

A sample of 50 trial trajectories are shown for closed and open-loop control in Figure 3. To show the evolution of the distribution of the trials, a series of 3σ covariance ellipses are drawn around the mean trajectory at equal increments along each flight segment and the spacecraft positions for each trial at these times are marked. The trajectories initially disperse from the starting distribution during the first diversion maneuver before decreases to meet the intermediate target covariance. Comparable open-loop trajectories are also shown in Figure 3 to give a reference of the effect of noise on the system. As expected, since the noise was zero-mean, the mean of the open-loop trajectories is nearly equivalent to the mean of the closed-loop trajectories. Similarly, plots of a selection of closed-loop trajectories over time are shown in Figure 4, and vehicle mass over time is shown in Figure 5. For this simulation, noise was only applied through Eq. (49), so variations in mass are the result of the feedback compensating for deviations from the nominal trajectory.

Controller feedback gains and the control magnitude, as a fraction of the maximum thrust of 18,000 N, are shown in Figure 6. At $t = 26$ s, there is a discontinuity in both feedback gains and control when the control law is changed for the second flight segment. While in this scenario the maximum thrust was not exceeded, there was not an explicit constraint on control magnitude. Thus, we had to tune the boundary conditions and total flight time until an admissible solution was obtained.

As a validation of the covariance evolution model, the variances in downrange position and altitude where computed over the 2,000 simulated trajectories and were compared to the variance predicted by Eq. (40). Figure 7 shows a nearly exact agreement at the initial and final time, but there is a minor deviation between the experimental and theoretical results around the mid-course of each flight segment. This is most likely due to the limited number of simulated trials or the assumption of fixing a prior mass profile.

VI. Conclusion

In this paper covariance steering theory was applied to the Martian powered descent problem, and was shown to successfully steer an initial to a target state mean and covariance without the need to tune weight

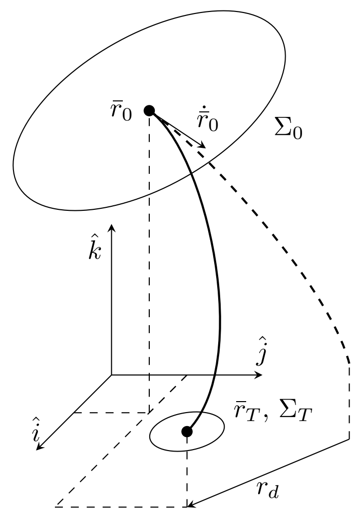

Figure 2. Divert guidance geometry. Given initial mean position, mean velocity, and covariance ($\bar{r}_0$, $\dot{\bar{r}}_0$, Σ_0), the spacecraft would follow an uncontrolled trajectory to $\tilde{r}(T)$. Powered descent guidance must steer the mean and covariance to ($\bar{r}_T$, Σ_T) with a requirement on divert radius r_d.

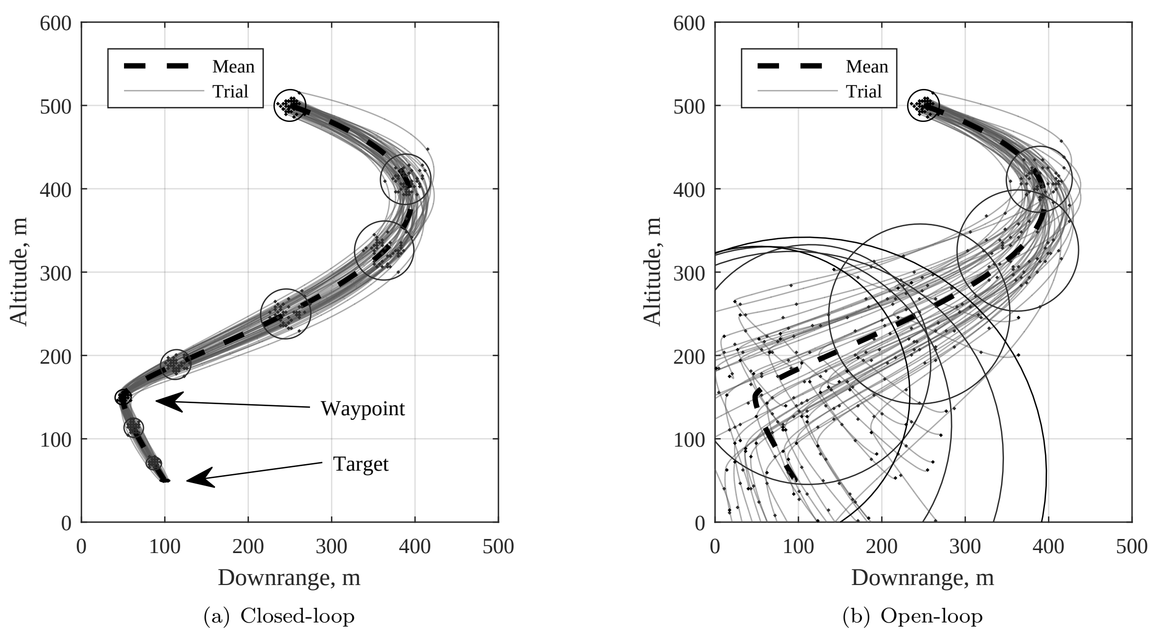

Figure 3. Simulated trajectories of a two-part divert maneuver. At the initial, intermediate target, and final target, the positions are marked and ellipse is drawn around a 95% confidence interval in black. Several points along the path are also marked to demonstrate how the trajectory dispersion changes with time.

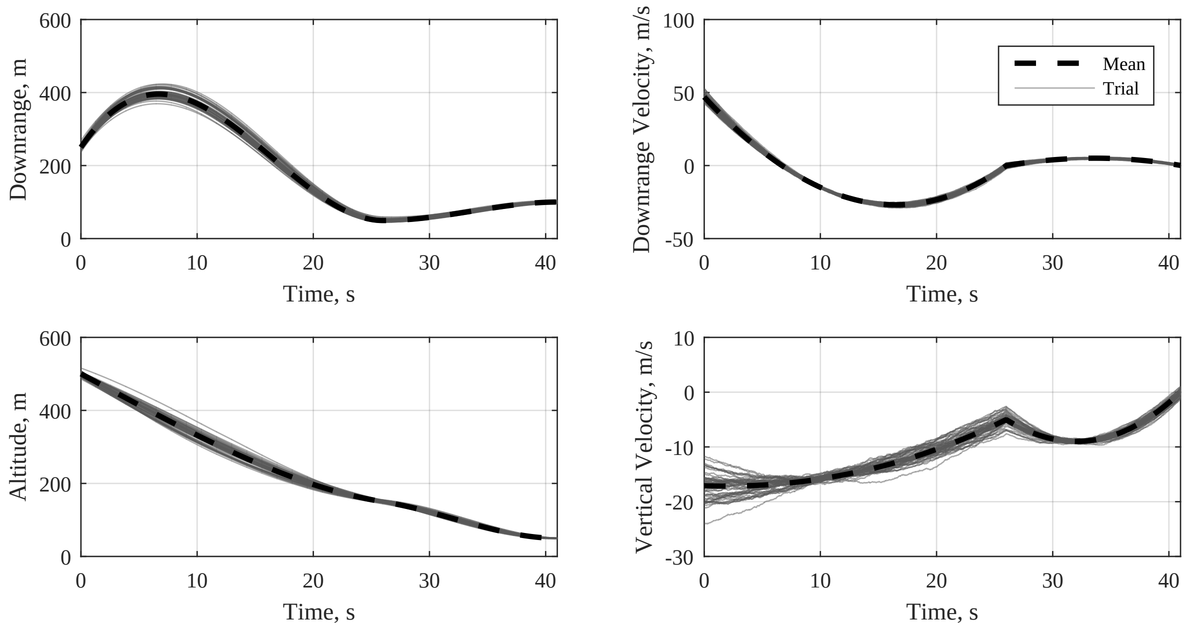

Figure 4. Downrange position, altitude, downrange velocity, and vertical velocity against time.

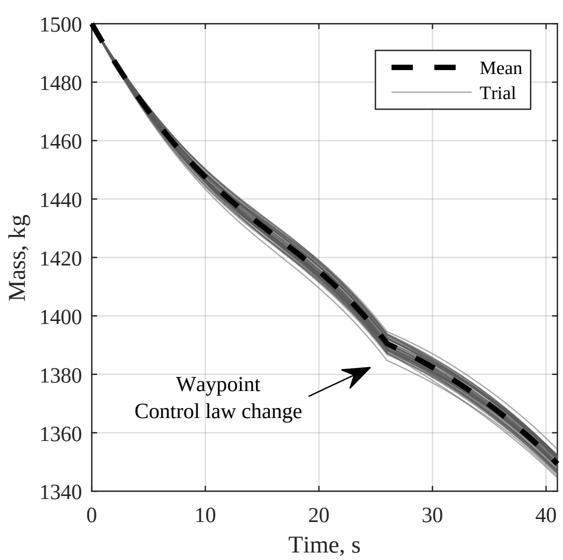

Figure 5. Vehicle mass against time.

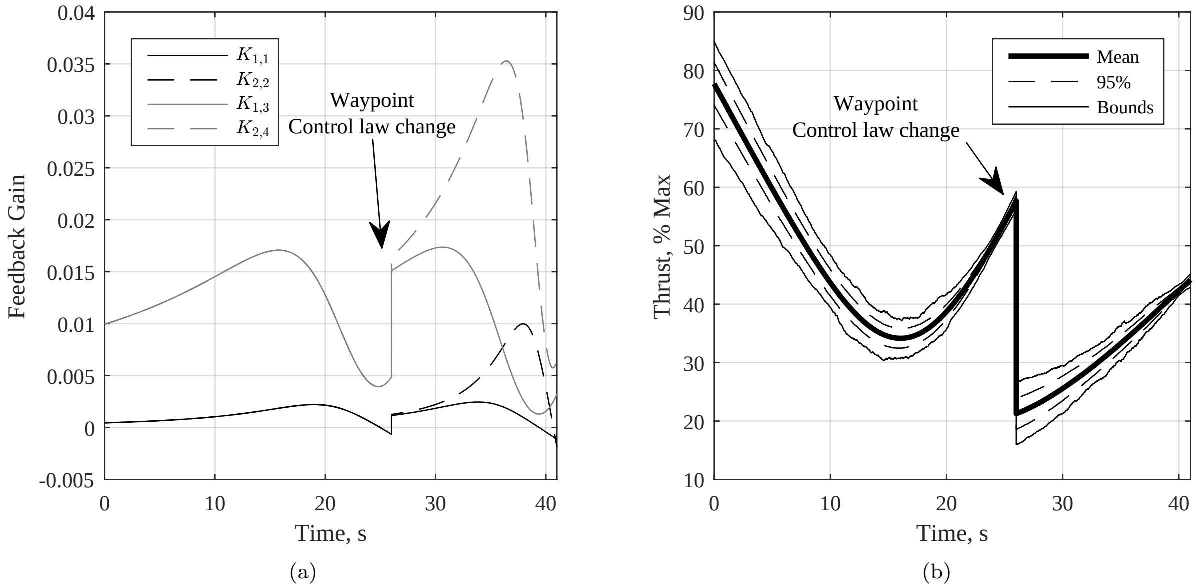

Figure 6. a) Feedback gains. Note that the change in target at $t = 26$ seconds. b) Mean, upper 95 percent, and maximum control magnitude over all trials.

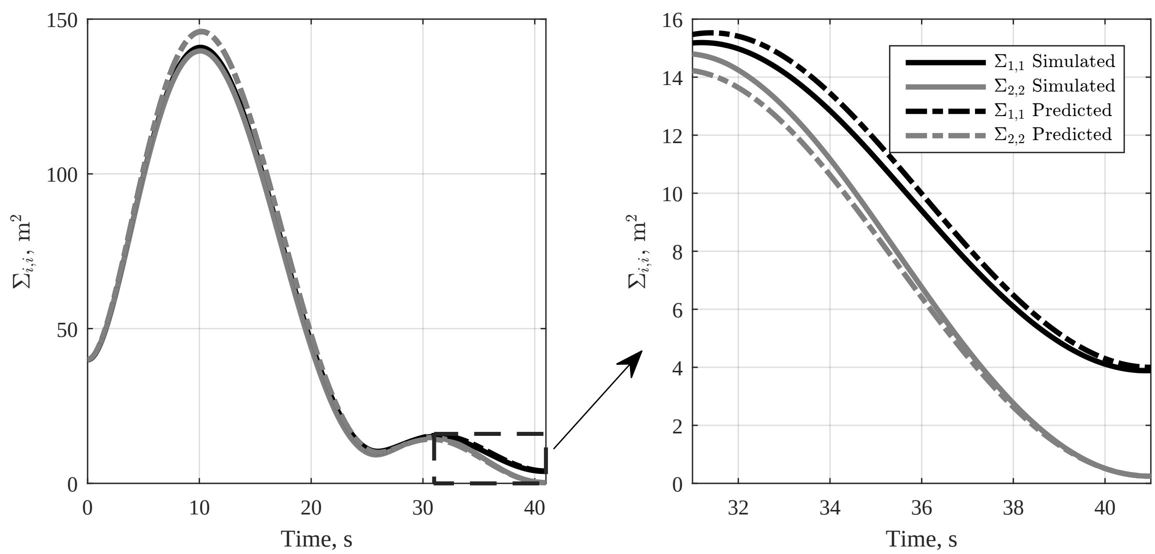

Figure 7. Comparison of predicted to measured variances of altitude and downrange position.

parameters, as is often the case with standard Monte Carlo approaches. Covariance steering theory was extended to include an affine forcing term to model gravitational acceleration and a scalar multiplier on noise magnitude was added to model the actual effect of nose. For the purposes of applying covariance steering theory to compute time-varying controller gains, the powered descent dynamic constraints were relaxed by replacing the relationship between thrust and mass flow rate with a prior mass profile. After using an iterative scheme to determine the prior mass profile, the proposed controller was effective in controlling the original nonlinear system.

Acknowledgment

This work has been supported in part by NASA Space Technology Research Fellowship award 80NSSC17K0093.

References

[1] National Aeronautics and Space Administration, *NASA Technology Roadmaps TA 9: Entry, Descent, and Landing Systems*, July 2015.

[2] R. N. Ingoldby, "Guidance and control system design of the viking planetary lander," *Journal of Guidance, Control, and Dynamics*, vol. 1, pp. 189–196, May 1978.

[3] D. A. Spencer and R. D. Braun, "Mars pathfinder atmospheric entry - trajectory design and dispersion analysis," *Journal of Spacecraft and Rockets*, vol. 33, no. 5, pp. 670–676, 1996.

[4] R. D. Braun and R. M. Manning, "Mars exploration entry, descent and landing challenges," in *2006 IEEE Aerospace Conference*, p. 18 pp., March 2006.

[5] P. Desai, J. Prince, E. Queen, R. Grover, and J. Cruz, "Entry, descent, and landing performance of the Mars phoenix lander," in *AIAA/AAS Astrodynamics Specialist Conference and Exhibit*, August 2008.

[6] S. W. Sell, J. L. Davis, A. M. S. Martin, and F. Serricchio, "Powered flight design and performance summary for the Mars science laboratory mission," *Journal of Spacecraft and Rockets*, vol. 51, no. 4, pp. 1197–1207, 2014.

[7] G. Singh, A. M. SanMartin, and E. C. Wong, "Guidance and control design for powered descent and landing on Mars," in *2007 IEEE Aerospace Conference*, pp. 1–8, March 2007.

[8] E. C. Wong, G. Singh, and J. P. Masciarelli, "Guidance and control design for hazard avoidance and safe landing on Mars," *Journal of Spacecraft and Rockets*, vol. 43, no. 2, pp. 378–384, 2006.

[9] A. A. Wolf, C. Graves, R. Powell, and W. Johnson, "Systems for pinpoint landing at Mars (AAS 04-272)," *Advances in Astronautical Sciences*, vol. 119, pp. 2677 – 2696, 2004.

[10] L. Blackmore, B. Açikmeşe, and D. P. Scharf, "Minimum-landing-error powered-descent guidance for Mars landing using convex optimization," *Journal of Guidance, Control, and Dynamics*, vol. 33, no. 4, pp. 1161–1171, 2010.

[11] R. Brockett, "Notes on the control of the liouville equation," in *Control of Partial Differential Equations*, (Berlin ; New York), Springer, 2010.

[12] Y. Chen, T. T. Georgiou, and M. Pavon, "Optimal steering of a linear stochastic system to a final probability distribution, Part I," *IEEE Transactions on Automatic Control*, vol. 61, pp. 1158–1169, May 2016.

[13] R. Brockett, "Control of partial differential equations," Lecture Notes in Mathematics ; 2048, (Berlin ; New York), CIME Course on Control of Partial Differential Equations (2010 : Cetrato, Italy), Springer, 2010.

[14] K. J. Åström, *Introduction to Stochastic Control Theory.* Mathematics in Science and Engineering. A Series of Monographs and Textbooks, Academic Press, 1970.

[15] J. Yong and X. Y. Zhou, *Stochastic Controls : Hamiltonian Systems and HJB Equations.* Applications of Mathematics: Stochastic Modeling and Applied Probability, New York: Springer, 1999.

[16] A. E. Bryson and Y.-C. Ho, *Applied Optimal Control; Optimization, Estimation, and Control.* Waltham, Mass.: Blaisdell Pub. Co., 1969.

[17] A. Wolf, J. Tooley, S. Ploen, M. Ivanov, B. Açikmeşe, and K. Gromov, "Performance trades for Mars pinpoint landing," in *2006 IEEE Aerospace Conference.*

[18] R. P. Kornfeld, R. Prakash, A. S. Devereaux, M. E. Greco, C. C. Harmon, and D. M. Kipp, "Verification and validation of the Mars science larorotary/ curiosity rover entry, descent, and landing system," *Journal of Spacecraft and Rockets*, vol. 51, no. 4, 2014.

[19] B. Açikmeşe, J. M. Carson III, and L. Blackmore, "Lossless convexification of nonconvex control bound and pointing constraints of the soft landing optimal control problem," *IEEE Transactions on Control Systems Technology*, vol. 21, no. 6, 2013.